

A Maximum Entropy Supervised Learning Algorithm for the Identification of Skin/Core Debonding in Honeycomb Aluminium Panels

V. Meruane, V. del Fierro and A. Ortiz-Bernardin
Department of Mechanical Engineering
Universidad de Chile, Santiago, Chile

Abstract

Honeycomb sandwich structures are used in a wide variety of applications. Nevertheless, due to manufacturing defects or impact loads, these structures can be subject to imperfect bonding or debonding between the skin and the honeycomb core. The presence of debonding reduces the bending stiffness of the composite panel, which causes detectable changes in its vibration characteristics. This paper presents a new supervised learning algorithm to identify debonded regions in aluminium honeycomb panels. The algorithm uses a linear approximation method handled by a statistical inference model based on the maximum-entropy principle. The merits of this new approach are twofold: training is avoided and data is processed in a period of time that is comparable to the one of neural networks. The honeycomb panels are modelled with finite elements using a simplified three-panel shell model. The adhesive layer between the skin and core is modelled using linear springs, the rigidities of which are reduced in debonded sectors. The algorithm is validated using experimental data of an aluminium honeycomb panel under different damage scenarios.

Keywords: sandwich structures, debonding, honeycomb, damage assessment, maximum entropy.

1 Introduction

The applications of sandwich structures continue to increase rapidly and range from satellites, aircraft, ships, automobiles, rail cars, wind energy systems and bridge construction, among others [1]. Sandwich panels typically consist of two thin face sheets or skins and a lightweight thicker core, which is sandwiched between two faces to

obtain a structure of superior bending stiffness. Nevertheless, due to manufacturing defects or impact loads, these structures can experience imperfect bonding or debonding between the skin and the honeycomb core. Debonding in a sandwich structure may severely degrade its mechanical properties, which can produce a catastrophic failure of the overall structure. Therefore, it is important to detect the presence of debonding at an early stage.

A disadvantage of sandwich structures is that their structural failures, especially in the core, cannot always be detected by traditional non-destructive detection methods. A global technique called vibration-based damage detection has been rapidly expanding over the last few years [2]. The basic idea is that vibration characteristics (natural frequencies, mode shapes, damping, frequency response function, etc.) are functions of the physical properties of the structure. Thus, changes to the material and/or geometric properties due to damage will cause detectable changes in the vibrations characteristics.

Jiang et al. [3] used a commercial finite element software to investigate the behaviour of debonded honeycomb structures. The honeycomb structure was modelled as a three-layer structure using 3D solid elements. The debonding between the skin and the core was modelled as a non-contacting area. Their results show that natural frequencies are sensitive indicators to the presence of debonding. Kim and Hwang [4] studied the effect of internal face-layer debonding in the natural frequencies and frequency response functions (FRFS) of a honeycomb beam. They use a continuous sandwich beam model to investigate the reduction in flexural-bending rigidity due to debonding of the sandwich beam. Their results reveal that the extent of the debonding plays an important role in determining the natural frequencies and mode shapes of the debonded sandwich beam. Burlayenko et al. [5, 6] studied the influence of skin/core debonding on the vibrations of honeycomb panels. The debonded region is modelled by creating a small gap between the face and the core. Spring elements were introduced between the double nodes in the debonded area. The authors investigated the influence of the debonding type, size, and location on the modal parameters of damaged sandwich panels with different boundary conditions. They concluded that the size of the debonded zone strongly influences the panel modal parameters; it reduces the natural frequencies and creates a discontinuity in the mode shapes. This influence is stronger for higher frequency modes. Mohanan et al. [7] studied the sensitivity of natural frequencies, mode shapes and modal strain energy to debonds and dents in metallic honeycomb beams. They used layered shell finite elements to model the beam. Their results indicate that natural frequencies and mode shapes are sensitive indicators to the presence of damage but less sensitive in identifying its location and size; modal strain energy was more effective in identifying the elements affected by the damage. Shahdin et al. [8] presented an experimental study on the effects of impact damage and core-only damage in honeycomb sandwich beams. Their results show that the damage produces a decrease in the natural frequency accompanied by an increase in the damping ratio. Furthermore, the damping ratio is a more sensitive parameter for damage detection than the natural frequencies, although it is much harder

to estimate it compared to the natural frequency.

Traditional vibration-based damage assessment approaches include the use of feed-forward neural networks. However, the slow learning speed of these networks and the large number of parameters that need to be tuned have been a major bottleneck in their application. Most of the damage assessment algorithms based on neural networks are restricted to problems where only a couple of variables need to be identified, such as the detection of a single crack over a beam. Islam and Craig [9] trained a back-propagation neural network with the first five natural frequencies of a composite beam to determine the location and size of any delamination. Natural frequencies were obtained through a modal analysis, which was performed using piezoceramic patches as both sensors and actuators. Back-propagation neural networks were used by Okafor et al. [10] to predict delamination size in composite beams based on changes in their natural frequencies. In this case, the delamination is assumed to be at the middle of the beam. The network was able to accurately predict dimensionless delamination sizes between 0.22 and 0.82 but under-predicted delamination sizes below 0.08. A similar approach is used by Valoor and Chandrashekhara [11] to predict delamination locations and sizes in a thick composite beam. They found that the errors were highest for delaminations located near the beam end and that in symmetrical structures, the network can only predict the possible location in each symmetrical segment. Hence, to locate the damage in symmetrical structures, more information, such as mode shapes, is needed. Ishak et al. [12] trained a multilayer perceptron network (MLP) to identify the location, depth and length of interfacial delamination in carbon/epoxy laminated composite beams. The network inputs are experimental displacement responses measured with a scanning laser vibrometer. Chakraborty [13] proposed a neural network approach to predict the size, shape and location of delamination in composite panels using natural frequencies. The method was validated using simulated data from a composite panel. The results show that the network works reasonably well when tested with unknown data. Nevertheless, the authors stated that the actual efficacy of the approach can be determined only when the network is trained and tested with experimental data. Su et al. [14] compared the efficiency of neural networks and genetic algorithms (GAs) for the evaluation of delaminations in composite beams based on the change in their natural frequencies. The response of the beams is measured using fibre Bragg grating sensors. The authors concluded that both algorithms are able to evaluate the delamination location, size and depth, but neural networks are more stable. Zhang et al. [15] examined three different inverse algorithms to predict the location and size of delamination in a composite beam: a direct solution using a graphical method, neural networks and surrogate optimisation based on GA. Their results show that the three algorithms can predict the delamination parameters, but neural networks are more sensitive to experimental noise.

A new nonparametric method for supervised learning is presented by Gupta et al. [16, 17]. This method generalizes linear approximation by using the maximum-entropy (max-ent) principle [18] for statistical inference. A similar approach is adopted by Erkan [19] for semi-supervised learning problems, where a decision rule is to

be learned from labeled and unlabeled data. By using max-ent methods, training is avoided and data is processed in a period of time that is comparable to the one of neural networks. In addition, it only requires one parameter to be selected. Hence, max-ent methods become very appealing for real-time health monitoring applications. Gupta [16] demonstrated the application of the max-ent approach to color management and gas pipeline integrity problems. In the present paper, we demonstrate the applicability of max-ent methods in structural damage assessment.

The primary contribution of this research is the development of a real-time damage assessment algorithm for honeycomb panels that uses a linear approximation method in conjunction with the mode shapes and natural frequencies of the structure. The linear approximation is handled by a statistical inference model based on the maximum-entropy principle [18]. The honeycomb panels are modelled with finite elements using a simplified three-panel shell model. The adhesive layer between the skin and core is modelled using linear springs, with reduced rigidities for the debonded sectors. The algorithm is validated using experimental data from an aluminium honeycomb panel containing different damage scenarios.

The remainder of this paper is structured as follows: Section 2 presents the proposed damage assessment algorithm and provides general antecedents and related research on the max-ent linear approximation method. Section 3 describes the construction of the numerical model for the honeycomb sandwich panel. Section 4 presents the experimental structure and the correlation between the experimental and numerical modes. Section 5 describes the setting up of the database. Sections 6 presents the case studies and the damage assessment results. Finally, conclusions and forthcoming work are presented in Section 7.

2 Damage assessment using linear approximation with maximum entropy

The main problem of vibration-based damage assessment is to ascertain the presence, location and severity of structural damage given a structure's dynamic characteristics. This principle is illustrated in Fig. 1; the vibration characteristics of the structure, which in this case correspond to mode shapes and natural frequencies, act as the input to the algorithm, and the outputs are the damage indices of each element in the structure.

Let the observation vector $\mathbf{Y}^i = \{Y_1^i, Y_2^i, \dots, Y_m^i\} \in \mathbb{R}^m$ represent the i th damage state of the structure, where m is the number of structural elements. Let the feature vector $\mathbf{X}^i = \{X_1^i, X_2^i, \dots, X_n^i\} \in \mathbb{R}^n$ represent a set of vibration characteristics of the structure associated with the damage state \mathbf{Y}^i .

The variables \mathbf{X} and \mathbf{Y} have joint distribution $P_{X,Y}$. Let a set of k independent and identically distributed samples be drawn from $P_{X,Y}$. These samples represent the database $(\mathbf{X}^1, \mathbf{Y}^1), (\mathbf{X}^2, \mathbf{Y}^2), \dots, (\mathbf{X}^k, \mathbf{Y}^k)$. The central problem in supervised learn-

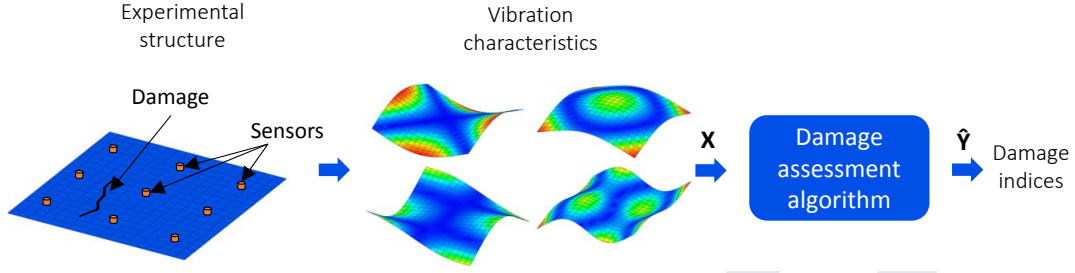


Figure 1: Principle of a vibration-based damage assessment algorithm.

ing is to form an estimate of $P_{Y|X}$, i.e. given a certain feature \mathbf{X} , estimate the corresponding observation \mathbf{Y} . Let $\hat{\mathbf{Y}}$ denote the estimated value of \mathbf{Y} . Linear approximation takes the N nearest neighbors to a test point \mathbf{X} and uses a linear combination of them to represent \mathbf{X} as

$$\mathbf{X} = \sum_{i=1}^N w_i(\mathbf{X}) \mathbf{X}^i(\mathbf{X}), \quad \sum_{i=1}^N w_i(\mathbf{X}) = 1, \quad (1)$$

where w_1, w_2, \dots, w_N are weighting functions, and $\mathbf{X}^1(\mathbf{X}), \mathbf{X}^2(\mathbf{X}), \dots, \mathbf{X}^N(\mathbf{X})$ are the N closest neighbors to a test point \mathbf{X} out of the database set. The equations given in (1) can be expressed as the following system of linear equations:

$$\mathbf{A}\mathbf{w} = \mathbf{b}, \quad \mathbf{w} \geq 0, \quad (2)$$

with $\mathbf{A} = \begin{bmatrix} X_1^1 & X_1^2 & \dots & X_1^N \\ X_2^1 & X_2^2 & \dots & X_2^N \\ \vdots & \vdots & \ddots & \vdots \\ X_n^1 & X_n^2 & \dots & X_n^N \\ 1 & 1 & \dots & 1 \end{bmatrix}_{(n+1) \times N}$, $\mathbf{b} = \begin{bmatrix} X_1 \\ X_2 \\ \vdots \\ X_n \\ 1 \end{bmatrix}_{(n+1) \times 1}$, $\mathbf{w} = \begin{bmatrix} w_1 \\ w_2 \\ \vdots \\ w_N \end{bmatrix}_{N \times 1}$.

After \mathbf{w} is obtained from (2), $\hat{\mathbf{Y}}$ is estimated as

$$\hat{\mathbf{Y}} = \sum_{i=1}^N w_i(\mathbf{X}) \mathbf{Y}^i(\mathbf{X}), \quad (3)$$

where $\mathbf{Y}^1(\mathbf{X}), \mathbf{Y}^2(\mathbf{X}), \dots, \mathbf{Y}^N(\mathbf{X})$ are the corresponding observations to the N selected neighbors. Typically, the system of equation (2) is undetermined, and its solution is tackled via a constrained optimization technique of the family of least-squares (nonnegative least-squares [20]). An alternative that provides the least-biased solution is obtained via the maximum-entropy (max-ent) variational principle [18]. Recently, max-ent methods have become quite popular in the computational mechanics community as a powerful tool for numerical solution of PDEs [21, 22, 23, 24, 25, 26, 26, 27, 28, 29], and their applications in the solution of ill-posed inverse problems have also been explored [30, 31].

The notion of entropy in information theory was introduced by Shannon as a measure of uncertainty [32]. Later, on using the Shannon entropy, Jaynes [18] postulated the maximum-entropy principle as a rationale means for least-biased statistical inference when insufficient information is available. The maximum-entropy principle is suitable to find the least-biased probability distribution when there are fewer constraints than unknowns and is posed as follows:

Consider a set of N discrete events $\{x_1, \dots, x_N\}$. The possibility of each event is $p_i = p(x_i) \in [0, 1]$ with uncertainty $-\ln p_i$. The Shannon entropy $H(p) = -\sum_{i=1}^N p_i \ln p_i$ is the amount of uncertainty represented by the distribution $\{p_1, \dots, p_N\}$. The least-biased probability distribution and the one that has the most likelihood to occur is obtained via the solution of the following optimization problem (maximum-entropy principle):

$$\max_{\mathbf{p} \in \mathbb{R}_+^N} - \sum_{i=1}^N p_i \ln p_i, \quad (4a)$$

subject to the constraints:

$$\sum_{i=1}^N p_i = 1, \quad \sum_{i=1}^N p_i g_r(x_i) = \langle g_r(x) \rangle, \quad (4b)$$

where \mathbb{R}_+^N is the non-negative orthant and $\langle g_r(x) \rangle$ is the expectation of the function $g_r(x)$.

The optimization problem (4) assigns probabilities to every x_i in the set. Now, assume that the probability p_i has an initial guess m_i known as a *prior*, which reduces its uncertainty to $-\ln p_i + \ln m_i = -\ln(p_i/m_i)$. An alternative problem can be formulated on using this *prior* in (4) [33]:

$$\max_{\mathbf{p} \in \mathbb{R}_+^n} - \sum_{i=1}^n p_i \ln \left(\frac{p_i}{m_i} \right), \quad (5a)$$

subject to the constraints:

$$\sum_{i=1}^n p_i = 1, \quad \sum_{i=1}^n p_i g_r(x_i) = \langle g_r(x) \rangle. \quad (5b)$$

In (5), the variational principle associated with $-\sum_{i=1}^n p_i \ln \left(\frac{p_i}{m_i} \right)$ is known as *the principle of minimum relative (cross) entropy* [34, 35]. Depending upon the *prior* employed, the optimization problem (5) will favor some x_i 's in the set by assigning more probability to them, and eventually, assigning non-zero probability ($p_i > 0$) to

a selected number of x_i ($i < N$) in the set. It can be easily seen that if the *prior* is constant, the Shannon-Jaynes entropy functional (4) is recovered as a particular case.

Due to its general character and flexibility, we adopt the relative entropy approach for our problem, where the probability p_i is replaced with the weighting function w_i of the linear approximation problem 1. This reads:

$$\max_{\mathbf{w} \in \mathbb{R}_+^N} \left[H(\mathbf{w}) = - \sum_{i=1}^N w_i(\mathbf{X}) \ln \left(\frac{w_i(\mathbf{X})}{m_i(\mathbf{X})} \right) \right], \quad (6a)$$

subject to the constraints:

$$\sum_{i=1}^N w_i(\mathbf{X}) \tilde{\mathbf{X}}^i = \mathbf{0}, \quad \sum_{i=1}^N w_i(\mathbf{X}) = 1, \quad (6b)$$

where $\tilde{\mathbf{X}}^i = \mathbf{X}^i - \mathbf{X}$ has been introduced as a shifted measure for stability purposes. A typical prior distribution is the smooth Gaussian [21]

$$m_i(\mathbf{X}) = \exp(-\beta_i \|\tilde{\mathbf{X}}^i\|^2), \quad (7)$$

where $\beta_i = \gamma/h_i^2$; γ is a parameter that controls the radius of the Gaussian prior at \mathbf{X}^i , and therefore its associated weight function; and h_i is a characteristic n -dimensional Euclidean distance between neighbors that can be distinct for each \mathbf{X}^i . In view of the optimization problem posed in (6) for supervised learning, maximizing the entropy chooses the weight solution that commits the least to any one in the database samples [17].

The solution of the max-ent optimization problem is handled by using the procedure of Lagrange multipliers, which yields [33]:

$$w_i(\mathbf{X}) = \frac{Z_i(\mathbf{X}; \boldsymbol{\lambda}^*)}{Z(\mathbf{X}; \boldsymbol{\lambda}^*)}, \quad Z_i(\mathbf{X}; \boldsymbol{\lambda}^*) = m_i(\mathbf{X}) \exp(-\boldsymbol{\lambda}^* \cdot \tilde{\mathbf{X}}^i), \quad (8)$$

where $Z(\mathbf{X}; \boldsymbol{\lambda}^*) = \sum_j Z_j(\mathbf{X}; \boldsymbol{\lambda}^*)$, $\tilde{\mathbf{X}}^i = [\tilde{X}_1^i \dots \tilde{X}_N^i]^T$ and $\boldsymbol{\lambda}^* = [\lambda_1^* \dots \lambda_N^*]^T$.

In (8), the Lagrange multiplier vector $\boldsymbol{\lambda}^*$ is the minimizer of the dual of the optimization problem posed in (6) [33]:

$$\boldsymbol{\lambda}^* = \arg \min_{\boldsymbol{\lambda} \in \mathbb{R}^N} \ln Z(\mathbf{X}; \boldsymbol{\lambda}), \quad (9)$$

which gives rise to the following system of nonlinear equations:

$$\mathbf{f}(\boldsymbol{\lambda}) = \nabla_{\boldsymbol{\lambda}} \ln Z(\boldsymbol{\lambda}) = - \sum_i^N w_i(\mathbf{X}) \tilde{\mathbf{X}}^i = \mathbf{0}, \quad (10)$$

where $\nabla_{\boldsymbol{\lambda}}$ stands for the gradient with respect to $\boldsymbol{\lambda}$. Once the converged $\boldsymbol{\lambda}^*$ is found, the weight functions are computed from (8).

3 Numerical model

Figure 2 shows a scheme for a honeycomb sandwich panel, consisting of two thin face sheets or skins and a honeycomb core, which are bonded together by an adhesive layer. The panel can be modelled by a detailed 3D finite element model, but the computational effort increases very rapidly as the number of cells increases. Therefore, it is more convenient to develop equivalent simplified models for the honeycomb core to reduce the required computational time.

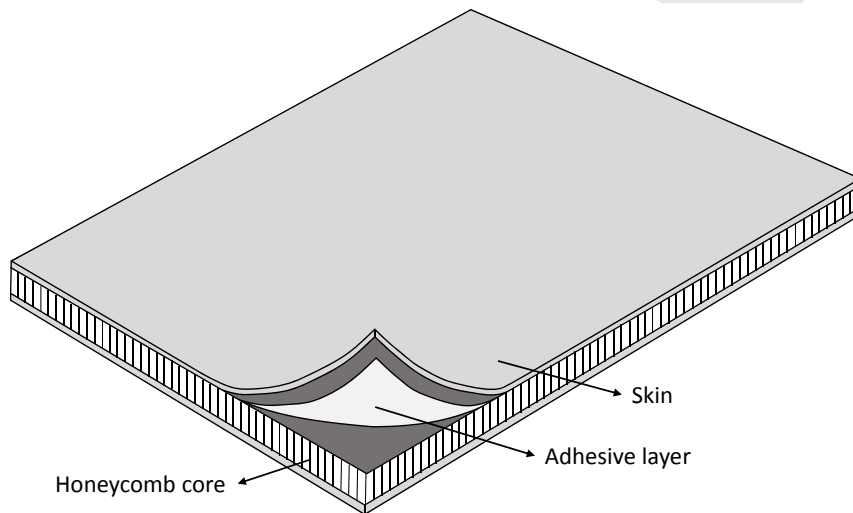


Figure 2: Scheme of a honeycomb sandwich panel.

Burton and Noor [36] studied the performance of nine different modelling approaches based on two-dimensional shell theories to predict the static response of sandwich panels. The results are compared to those from a detailed three-dimensional model. Their study showed that the global response can be accurately predicted by discrete three-layer models, predictor-corrector approaches and even first-order shear deformation theory, provided that proper values for the shear correction factors are used. According to Birman and Bert [37], a key factor in the practical application of the first-order shear deformation theory is the determination of the shear correction factor. The analysis presented by these researchers concluded that the shear correction factor should be taken with a value equal to unity for sandwich structures, as a first approximation. The work presented by Burton and Noor [38] showed that continuum layer models for the honeycomb core provide solutions that are close to those calculated by using detailed finite element models. Tanimoto et al. [39] used beam elements to model the honeycomb core and the adhesive layer. The proposed model was validated by experimental vibration tests. Burlayenko and Sadowski [40] performed an analysis of sandwich plates with hollow and foam-filled honeycomb cores using a commercially available finite element code. The sandwich plates were modelled on the basis of a simplified three-layered continuum model using a mixed shell/solid approach. Consequently, the prediction of the dynamic response of the honeycomb

panels can be accomplished by equivalent continuum models. In the present study, the honeycomb panels are modelled with finite elements using a simplified three-panel shell model and the adhesive layer between the skin and core is modelled using linear springs. Because the properties of the skin are known, the attention is focused on modelling the effective properties of the adhesive layer and the core material.

A debonded region between the skin and core of a honeycomb panel is similar to a delamination in laminated composites. There are a considerable amount of analytical and numerical methods used to model delaminated composite laminates. Della and Shu [41] provide an extensive review of them. The majority of these methods can be categorised into two classes. The first is a region approach where the laminate is divided into sub-laminates and continuity conditions are imposed at the junctions, whereas the second is a layer-wise model where delamination is introduced as an embedded layer or as a discontinuity function in the displacement field. On the other hand, modelling vibrations in sandwich structures with debonding is generally accompanied by contact problems between the interfaces of the debonded region [42]. Burlayenko and Sadowski [5, 6] modelled the debonded region by creating a small gap between the face and the core and by introducing bi-linear spring elements between the double nodes in the debonded area. The springs have a stiffness equal to zero in tension and a large value in compression, simulating a contact condition. A piecewise-linear model does not predict a unique mode shape as in a linear system, but the mode shape depends on the vibration amplitude. In this study, the adhesive layer between the skin and core is modelled using linear springs, with reduced rigidity in debonded sectors, as shown in Fig. 3.

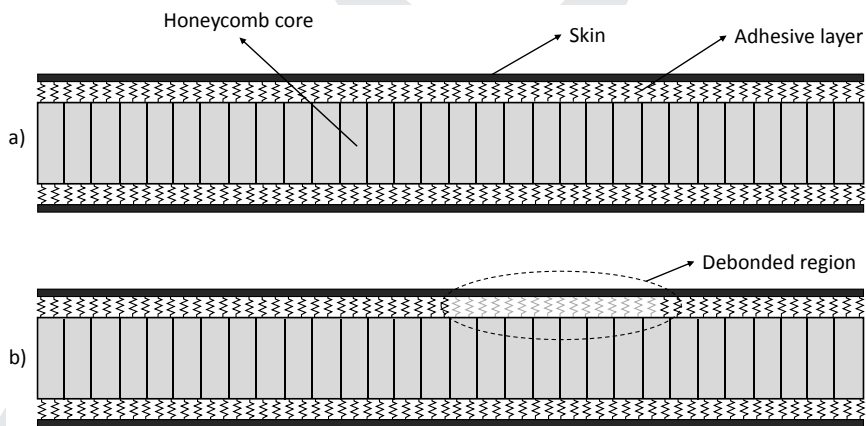


Figure 3: Lateral view of the numerical model: a) undamaged panel, b) panel with a debonded region.

The numerical model is built in `Matlab`[®] using the `SDTools` Structural Dynamics Toolbox [43], the skins and honeycomb panel are modelled with standard isotropic 4-node shell elements. The final model shown in Fig. 4 has 10,742 shell and 7,242 spring elements. The mechanical properties of the sandwich construction depend upon the adhesives, temperature and pressure used during curing. In addition, the anisotropic

nature of the honeycomb core makes testing the sandwich specimens mandatory to determine their properties with accuracy. Here, the mechanical properties of the adhesive layer and the honeycomb core are determined by updating the finite element model with the experimental mode shapes and natural frequencies for both undamaged cases and those with debonding.

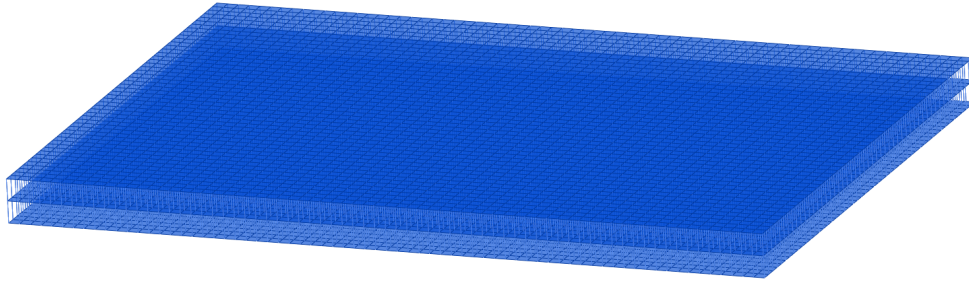


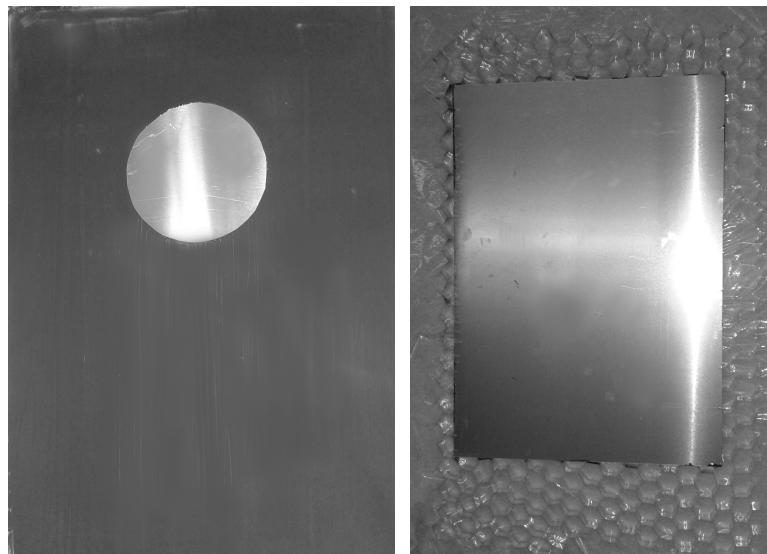
Figure 4: Finite element model of the sandwich panel.

4 Experimental structure

The experimental structure consists of a sandwich panel of $0.25 \times 0.35 \text{ m}^2$ made of an aluminium honeycomb core bonded to two aluminium skins, each with a thickness of 0.8 mm . The properties of the core are summarised in Table 1. The skins are bonded to the honeycomb core using an epoxy adhesive that provides a high performance solution to ambient temperature cure bonding of aluminium honeycomb to a wide range of skin materials. Figure 5(a) shows an aluminium sheet with a layer of epoxy adhesive, the circular region without adhesive is introduced to simulate debonding. To ensure perfect bonding, the panel is cured using a vacuum bagging system, as shown in Fig. 5(b).

Cell size	19.1 mm
Foil thickness	$5 \times 10^{-5} \text{ m}$
Thickness	10 mm
Density	20.8 kg/m^3
Compressive strength	0.448 MPa
Shear strength in longitudinal direction (σ_{xy})	0.345 MPa
Shear modulus in longitudinal direction (G_{xy})	89.63 MPa
Shear strength in width direction (σ_{yz})	0.241 MPa
Shear modulus in width direction (G_{yz})	41.37 MPa

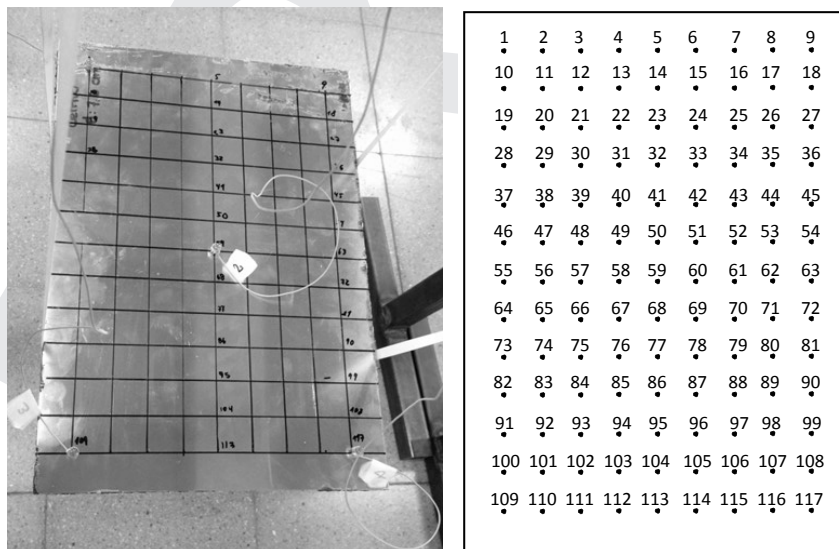
Table 1: Properties of the honeycomb core



(a) layer of epoxy adhesive over the skin (b) vacuum bagging of the panel

Figure 5: Fabrication of the experimental panel

Figure 6 shows the experimental setup used to simulate a free boundary condition. The honeycomb sandwich panel is suspended by soft elastic bands. The out of plane vibration is captured by four miniature piezoelectric accelerometers located in three corners and in the centre of the panel. The panel is excited by an impact hammer at the 117 points described in Fig. 6(b), resulting in 468 measured Frequency Response Functions.



(a) panel suspended by elastic bands (b) distribution of measurement point

Figure 6: Experimental set-up

The identified modal parameters of the experimental structure are used to update the numerical model. The parameters that were updated in the numerical model are the following: the density and Young's Modulus of the skins; the density, bending stiffness and shear correction factor of the core; and the stiffness of the springs representing the adhesive layer.

Figure 7 shows the first six experimental mode shapes compared to those from the numerical model after updating. The correlation between two mode shapes is measured by the Modal Assurance Criterion (MAC). The results show that the correlation between the numerical and experimental modes is almost perfect for the first three modes, with MAC values higher than 0.99. The fifth mode presents the lowest correlation, with a MAC value of 0.83. In this case, the first-order shear approximation may not be sufficient. The maximum difference between the experimental and the numerical natural frequencies is 11%.

Figure 8 presents the correlation between the numerical and experimental modes for the case with a circular debonded region at the centre of the plate. The modes are plotted over the surface of the debonded skin. Here, the numerical model was updated again considering the spring stiffness in the debonded region as updating parameter. Although the correlation is not as good as in the undamaged case, both the numerical and experimental models show the same behaviour in the presence of damage, which is a reduction in the natural frequencies, and a strong discontinuity at the debonded region for mode 3.

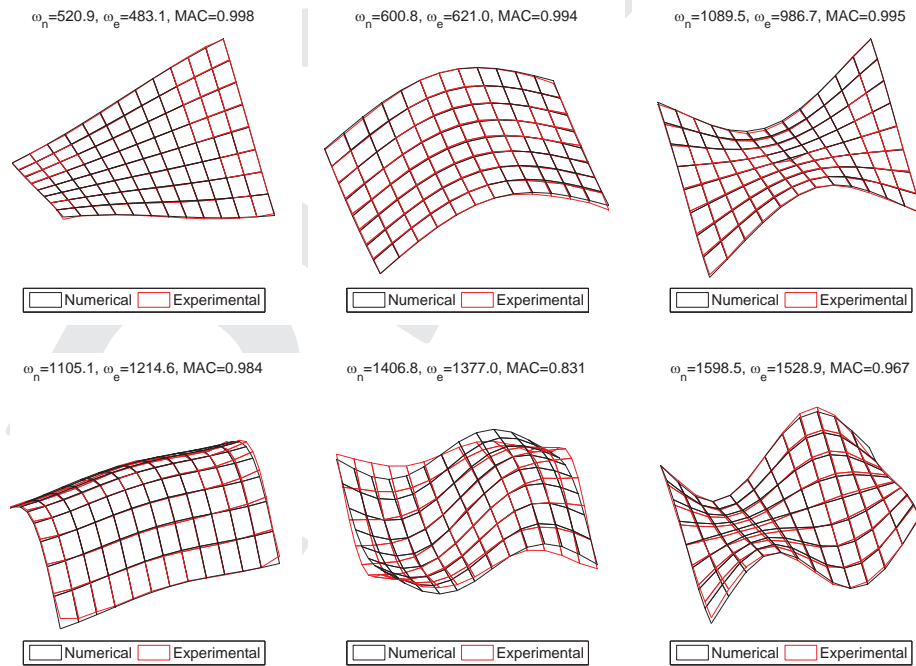


Figure 7: Numerical and experimental undamaged mode shapes.

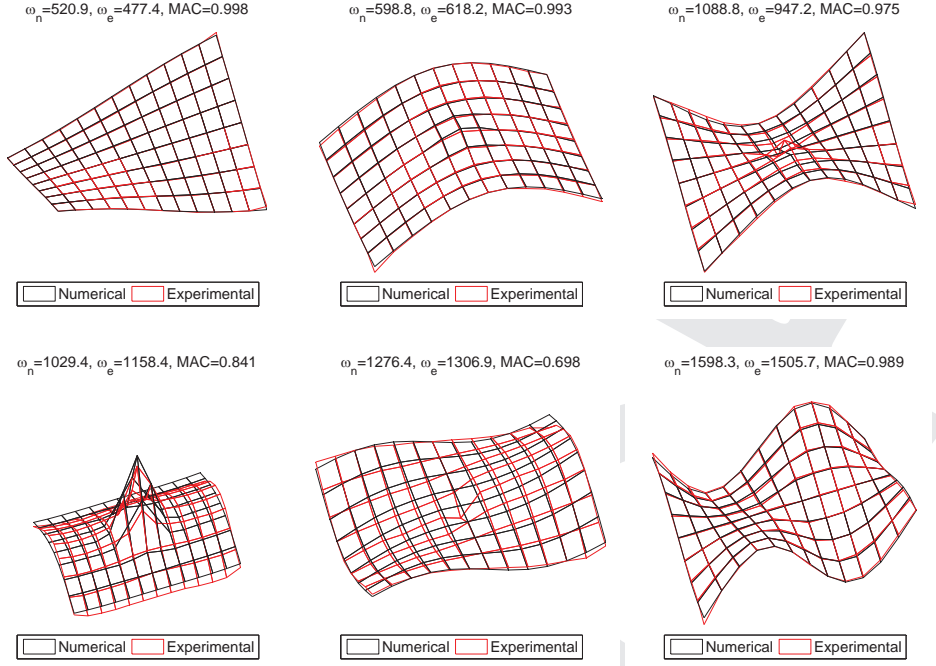


Figure 8: Numerical and experimental mode shapes with a debonded region at the center of the panel.

5 Construction of the database

Database samples are generated using the numerical model of the structure. The database contains mode shape and natural frequencies changes associated to different damage scenarios, which are used to assess the experimental damage. The patterns are generated by considering single damage scenarios with thirteen debonded radius equally distributed between 0.01 and 0.07 m.

5.1 Feature vector

The j th feature vector \mathbf{X}^j contains the experimental changes in the natural frequencies and mode shapes with respect to the intact case:

$$\mathbf{X}^j = \left\{ \begin{array}{c} \left(\frac{\omega^D - \omega^U}{\omega} \right)^2 \\ \frac{\sum_j (\phi_j^D - \phi_j^U)^2}{\max(\sum_j (\phi_j^D - \phi_j^U)^2)} \end{array} \right\}, \quad (11)$$

where ω represents a vector containing the natural frequencies and ϕ_j represents the i th mode shape vector. The superscripts D and U refer to damaged and undamaged, respectively. The vector of the mode shape changes is normalised with respect to

its maximum value to reduce the difference between the numerical and experimental results. This difference is because the numerical model does not contain contact conditions whereas the experimental model does.

5.2 Observation vector

Damage is modelled by circular-shaped debonded regions centred at some of the 117 points presented in Fig. 6(b). Debonding is restricted to the skin that is measured during experiments. The j th observation vector is represented by $\mathbf{Y}^j = \{Y_1^j, Y_2^j, \dots, Y_{117}^j\}$, where the value $Y_i^j > 0$ implies a debonded region with a radius Y_i^j centered at the i th point, whereas a value $Y_i^j = 0$ indicates that the i th point is undamaged.

6 Damage assessment results

The algorithm is tested for the three damage scenarios shown in Fig. 9. The first case has a debonded region centred at point 59 (the centre of the panel), the second case has a debonded region centred somewhere between points 30, 31, 39 and 40, and the third case has a debonded region centred between points 31, 32, 40, 41. The radius for the three debonded regions are 0.038, 0.039 and 0.045 respectively.

Two approaches are used to solve the linear approximation problem presented in equation (1): max-ent and nonnegative least-squares. In both cases, the solution is obtained by using the closest ten neighbors to the test point. The time needed to assess damage is 0.7 and 0.03 seconds for the max-ent and nonnegative least-squares approaches respectively.

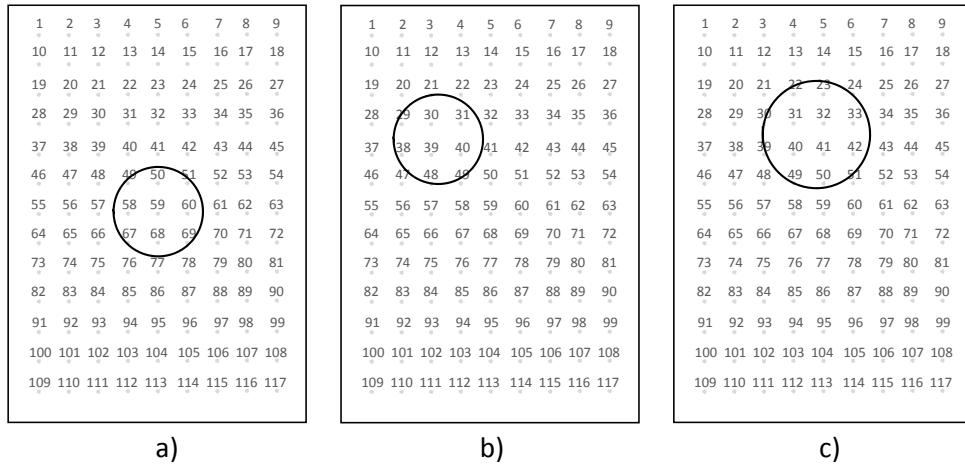


Figure 9: Experimental damage scenarios introduced to the panel; the circles indicate the debonded regions.

Figures 10, 11 and 12 present the damage assessment results. The damage detected

is represented as a black region where each pixel represents a debonded spring. The actual damage introduced into the panel is presented as a circle. In the three cases, the max-ent approach identifies debonded regions that are closer to the actual damage when compared to the least-squares method. In the first case, the centre of the experimental damage matches one of the 117 predefined positions. Thus, the max-ent algorithm is able to detect the exact position of the debonded region. However, when the actual centre of the damage does not match one of the 117 positions, as in the second and third cases, the algorithm detects the damage at a position that is close to the actual location but not at the exact position.

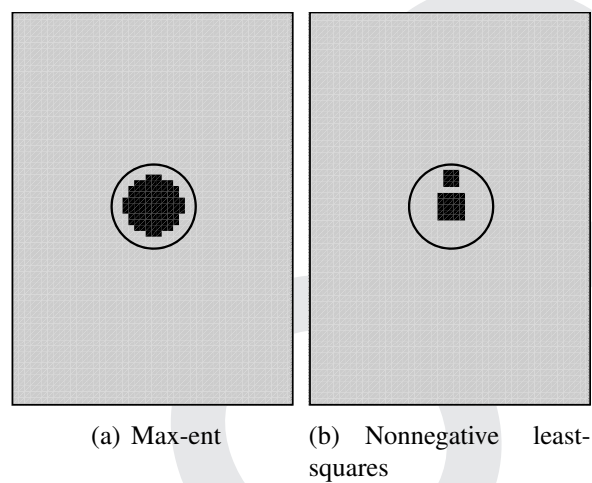


Figure 10: Damage assessment results for the first damage scenario

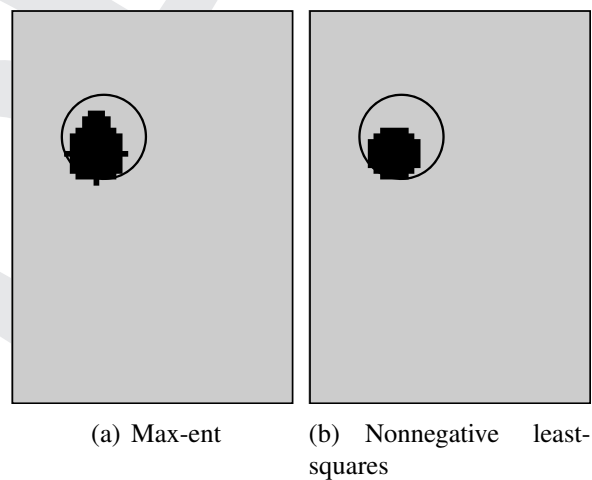


Figure 11: Damage assessment results for the second damage scenario

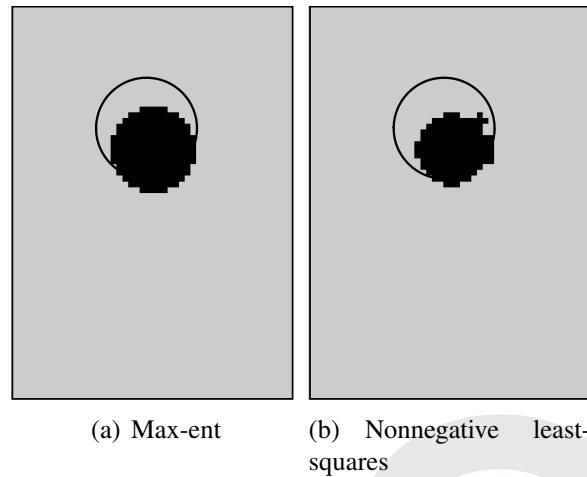


Figure 12: Damage assessment results for the third damage scenario

7 Conclusions

This paper presented a new methodology to identify debonded regions in aluminium honeycomb panels using a linear approximation method handled by a statistical inference model based on the maximum-entropy principle. The algorithm was validated using experimental data from an aluminium honeycomb panel subjected to different damage scenarios.

The honeycomb panels were modelled with finite elements using a simplified three-panel shell model. The adhesive layer between the skin and core was modelled using linear springs, with the rigidity reduced in debonded sectors. This numerical model was able to predict with reasonable accuracy the first six modes of the undamaged and damaged panel. Nevertheless, the numerical model can be improved by using higher order shear approximations.

In the three experimental cases, the linear approximation using the max-ent technique was successful in assessing the experimental damage. The detected damage closely corresponds to the experimental damage in all cases. In addition, the damage state of the panels is assessed in less than one second, thus providing the possibility of continuously monitoring their condition. Further research is needed to adapt this algorithm to cases with multiple debonded regions and to test its performance with more complex configurations.

Acknowledgments

Valentina del Fierro was supported by CONICYT grant CONICYT-PCHA/ Magster Nacional/2013-221320691. The authors acknowledge the partial financial support of the Chilean National Fund for Scientific and Technological Development (Fondecyt)

under Grants No. 11110389 and 11110046.

References

- [1] J.R. Vinson, “Sandwich structures: past, present, and future”, in *Sandwich Structures 7: Advancing with Sandwich Structures and Materials*, pages 3–12. Springer, 2005.
- [2] E. Carden, P. Fanning, “Vibration Based Condition Monitoring: A Review”, *Structural Health Monitoring*, 3(4): 355–377, 2004.
- [3] L. Jiang, K. Liew, M. Lim, S. Low, “Vibratory behaviour of delaminated honeycomb structures: a 3-D finite element modelling”, *Computers & Structures*, 55(5): 773–788, 1995.
- [4] H.Y. Kim, W. Hwang, “Effect of debonding on natural frequencies and frequency response functions of honeycomb sandwich beams”, *Composite Structures*, 55(1): 51–62, 2002.
- [5] V. Burlayenko, T. Sadowski, “Dynamic behaviour of sandwich plates containing single/multiple debonding”, *Computational Materials Science*, 50(4): 1263–1268, 2011.
- [6] V.N. Burlayenko, T. Sadowski, “Influence of skin/core debonding on free vibration behavior of foam and honeycomb cored sandwich plates”, *International Journal of Non-Linear Mechanics*, 45(10): 959–968, 2010.
- [7] A. Mohanan, K. Pradeep, K. Narayanan, “Performance Assessment of Sandwich Structures with Debonds and Dents”, *International Journal of Scientific & Engineering Research*, 4(5): 174–179, 2013.
- [8] A. Shahdin, J. Morlier, Y. Gourinat, “Damage monitoring in sandwich beams by modal parameter shifts: A comparative study of burst random and sine dwell vibration testing”, *Journal of Sound and Vibration*, 329(5): 566–584, 2010.
- [9] A.S. Islam, K.C. Craig, “Damage detection in composite structures using piezoelectric materials (and neural net)”, *Smart Materials and Structures*, 3: 318–328, 1994.
- [10] A.C. Okafor, K. Chandrashekhara, Y. Jiang, “Delamination prediction in composite beams with built-in piezoelectric devices using modal analysis and neural network”, *Smart Materials and Structures*, 5(3): 338–347, 1996.
- [11] M.T. Valoor, K. Chandrashekhara, “A thick composite-beam model for delamination prediction by the use of neural networks”, *Composites science and technology*, 60(9): 1773–1779, 2000.
- [12] S. Ishak, G. Liu, H. Shang, S. Lim, “Locating and sizing of delamination in composite laminates using computational and experimental methods”, *Composites Part B: Engineering*, 32(4): 287–298, 2001.
- [13] D. Chakraborty, “Artificial neural network based delamination prediction in laminated composites”, *Materials & Design*, 26(1): 1–7, 2005.
- [14] Z. Su, H.Y. Ling, L.M. Zhou, K.T. Lau, L. Ye, “Efficiency of genetic algorithms and artificial neural networks for evaluating delamination in composite structures

- using fibre Bragg grating sensors”, *Smart Materials and Structures*, 14(6): 1541–1553, 2005.
- [15] Z. Zhang, K. Shankar, T. Ray, E.V. Morozov, M. Tahtali, “Vibration-Based Inverse Algorithms for Detection of Delamination in Composites”, *Composite Structures*, 102: 226–236, 2013.
- [16] M.R. Gupta, *An information theory approach to supervised learning*, PhD thesis, Stanford University, 2003.
- [17] M.R. Gupta, R.M. Gray, R.A. Olshen, “Nonparametric supervised learning by linear interpolation with maximum entropy”, *Pattern Analysis and Machine Intelligence, IEEE Transactions on*, 28(5): 766–781, 2006.
- [18] E.T. Jaynes, “Information theory and statistical mechanics”, *Physical Review*, 106(4): 620–630, 1957.
- [19] A.N. Erkan, *Semi-supervised learning via generalized maximum entropy*, PhD thesis, New York University, 2010.
- [20] C.L. Lawson, R.J. Hanson, *Solving least squares problems*, Volume 161, SIAM, 1974.
- [21] M. Arroyo, M. Ortiz, “Local maximum-entropy approximation schemes: a seamless bridge between finite elements and meshfree methods”, *International Journal for Numerical Methods in Engineering*, 65(13): 2167–2202, 2006.
- [22] A. Ortiz, M.A. Puso, N. Sukumar, “Maximum-entropy meshfree method for compressible and near-incompressible elasticity”, *Computer Methods in Applied Mechanics and Engineering*, 199(25-28): 1859–1871, 2010.
- [23] L.L. Yaw, N. Sukumar, S.K. Kunnath, “Meshfree co-rotational formulation for two-dimensional continua”, *International Journal for Numerical Methods in Engineering*, 79(8): 979–1003, 2009.
- [24] C.J. Cyron, M. Arroyo, M. Ortiz, “Smooth, second order, non-negative mesh-free approximants selected by maximum entropy”, *International Journal for Numerical Methods in Engineering*, 79(13): 1605–1632, 2009.
- [25] A.M. Rosolen, R.D. Millán, M. Arroyo, “On the optimum support size in mesh-free methods: a variational adaptivity approach with maximum entropy approximants”, *International Journal for Numerical Methods in Engineering*, 82(7): 868–895, 2010.
- [26] D. González, E. Cueto, M. Doblaré, “A higher order method based on local maximum entropy approximation”, *International Journal for Numerical Methods in Engineering*, 83(6): 741–764, 2010.
- [27] B. Li, F. Habbal, M. Ortiz, “Optimal transportation meshfree approximation schemes for fluid and plastic flows”, *International Journal for Numerical Methods in Engineering*, 83(12): 1541–1579, 2010.
- [28] C. Cyron, K. Nissen, V. Gravemeier, W. Wall, “Stable meshfree methods in fluid mechanics based on Green’s functions”, *Computational Mechanics*, 46: 287–300, 2010.
- [29] C. Cyron, K. Nissen, V. Gravemeier, W. Wall, “Information flux maximum-entropy approximation schemes for convection and diffusion problems”, *International Journal for Numerical Methods in Fluids*, 64: 1180–1200, 2010.

- [30] F. Gamboa, E. Gassiat, “Bayesian methods and maximum entropy for ill-posed inverse problems”, *The Annals of Statistics*, 25(1): 328–350, 1997.
- [31] J.M. Loubes, B. Pelletier, “Maximum entropy solution to ill-posed inverse problems with approximately known operator”, *Journal of Mathematical Analysis and Applications*, 344(1): 260–273, 2008.
- [32] C.E. Shannon, “A mathematical theory of communication”, *The Bell Systems Technical Journal*, 27: 379–423, 1948.
- [33] N. Sukumar, R.W. Wright, “Overview and construction of meshfree basis functions: from moving least squares to entropy approximants”, *International Journal for Numerical Methods in Engineering*, 70(2): 181–205, 2007.
- [34] S. Kullback, *Information Theory and Statistics*, Wiley, New York, NY, 1959.
- [35] J.E. Shore, R.W. Johnson, “Axiomatic derivation of the principle of maximum entropy and the principle of minimum cross-entropy”, *IEEE Transactions on Information Theory*, 26(1): 26–36, 1980.
- [36] W.S. Burton, A.K. Noor, “Assessment of computational models for sandwich panels and shells”, *Computer Methods in Applied Mechanics and Engineering*, 124(1): 125–151, 1995.
- [37] V. Birman, C.W. Bert, “On the choice of shear correction factor in sandwich structures”, *Journal of Sandwich Structures and Materials*, 4(1): 83–95, 2002.
- [38] W. Burton, A. Noor, “Assessment of continuum models for sandwich panel honeycomb cores”, *Computer Methods in Applied Mechanics and Engineering*, 145(3): 341–360, 1997.
- [39] Y. Tanimoto, T. Nishiwaki, T. Shiomi, Z. Maekawa, “A numerical modeling for eigenvibration analysis of honeycomb sandwich panels”, *Composite Interfaces*, 8(6): 393–402, 2001.
- [40] V.N. Burlayenko, T. Sadowski, “Analysis of structural performance of sandwich plates with foam-filled aluminum hexagonal honeycomb core”, *Computational Materials Science*, 45(3): 658–662, 2009.
- [41] C.N. Della, D. Shu, “Vibration of delaminated composite laminates: A review”, *Applied Mechanics Reviews*, 60(1): 1–20, 2007.
- [42] I. Müller, “Clapping in delaminated sandwich-beams due to forced oscillations”, *Computational Mechanics*, 39(2): 113–126, 2007.
- [43] SDTools, “Structural dynamics toolbox & FEMLink”, *Users Guide Version*, 2014.